nature cell biology

p53 regulates glucose metabolism through an IKK–NF-κB pathway and inhibits cell transformation

Keiko Kawauchi[1], Keigo Araki[1], Kei Tobiume[1] and Nobuyuki Tanaka[1,2]

Cancer cells use aerobic glycolysis preferentially for energy provision[1,2] and this metabolic change is important for tumour growth[3,4]. Here, we have found a link between the tumour suppressor p53, the transcription factor NF-κB and glycolysis. In p53-deficient primary cultured cells, kinase activities of IKKα and IKKβ and subsequent NF-κB activity were enhanced. Activation of NF-κB, by loss of p53, caused an increase in the rate of aerobic glycolysis and upregulation of *Glut3*. Oncogenic Ras-induced cell transformation and acceleration of aerobic glycolysis in p53-deficient cells were suppressed in the absence of p65/NF-κB expression, and were restored by GLUT3 expression. It was also shown that a glycolytic inhibitor diminished the enhanced IKK activity in p53-deficient cells. Moreover, in Ras-expressing p53-deficient cells, IKK activity was suppressed by p65 deficiency and restored by GLUT3 expression. Taken together, these data indicate that p53 restricts activation of the IKK–NF-κB pathway through suppression of glycolysis. These results suggest that a positive-feedback loop exists, whereby glycolysis drives IKK–NF-κB activation, and that hyperactivation of this loop by loss of p53 is important in oncogene-induced cell transformation.

Increased dependence on glycolysis for ATP synthesis instead of oxidative phosphorylation in the presence of oxygen is known as the Warburg effect[1]. This effect is observed in many cancer cells and the metabolic shift to a higher rate of glycolysis can be seen clinically by positron emission tomography (PET)[5]. The most frequently mutated gene in human cancer cells is *p53* (ref. 6), which functions as a transcriptional activator and exerts its biological activity by inducing expression of its target genes[7]. Primary cultured cells from p53-deficient ($p53^{-/-}$) mice are easily transformed by a diverse range of oncogenes[8,9]. Recently, it was reported that activation of oncogenes such as *ras* trigger DNA-damage responses, inducing apoptosis or senescence through a p53-dependent pathway in normal cells[10,11]. Thus, oncogene-induced transformation is suppressed by p53-mediated surveillance, resulting in the elimination of cells with activated oncogenes. However, the specific mechanisms involved in the acquisition by oncogenes in p53-deficient cells of an anchorage-independent growth advantage, a hallmark of transformed cells, remain unclear. Numerous studies have demonstrated that constitutive activation of NF-κB is frequently observed in many types of cancer cells and that NF-κB has an important role in oncogenesis[12,13]. These findings indicate that p53 suppresses NF-κB activation and regulates oncogene-induced transformation; however this remains controversial[14–17].

To investigate the role of p53 in the regulation of NF-κB activity, we first examined the activity of NF-κB in $p53^{-/-}$ mouse embryonic fibroblasts (MEFs). The transcriptional and DNA-binding activities of NF-κB were enhanced in $p53^{-/-}$MEFs (Fig. 1a–c). As activation of NF-κB is achieved through the action of IKK, it was considered that IKKα/β activity was enhanced in $p53^{-/-}$MEFs. We found that phosphorylation of the active sites of IKKα/β was markedly increased in $p53^{-/-}$MEFs, compared with wild-type MEFs (Fig. 1d). The enhanced DNA-binding activity of NF-κB was abolished by knockdown of IKKα or IKKβ using short interfering (si) RNA (Fig. 1e), indicating that the IKK–NF-κB pathway is activated in $p53^{-/-}$MEFs. We next investigated whether NF-κB activation affects oncogene-induced cell transformation in $p53^{-/-}$MEFs (that is, acquisition of a growth advantage in soft agar). The activated form of Ha–Ras (Ha–RasV12) could induce cell transformation in $p53^{-/-}$MEFs, whereas it was hardly observed in $p53^{-/-}p65^{-/-}$MEFs (Fig. 1f, h, bottom panel). In the presence of Ha–RasV12, the growth rate (Fig. 1g) and morphology of MEFs (Fig. 1h, top panel) in monolayer cultures were virtually unchanged. We also performed *p65* knockdown using siRNA in $p53^{-/-}$MEFs and obtained similar results as those for $p53^{-/-}p65^{-/-}$MEFs (Fig. 1i, j). Thus, we showed that NF-κB has an essential role in oncogene-induced cell transformation in $p53^{-/-}$MEFs.

It has been reported that p53 activation causes downregulation of several glycolysis-regulating factors such as the glycolytic enzyme phosphoglycerate mutase (PGM)[18], and the glucose transporter (GLUT)[19]. Furthermore, p53 activation leads to an increased rate of mitochondrial respiration by inducing expression of SCO2 (synthesis of cytochrome oxidase 2)[20]. Thus, the rate of glycolysis is increased and the rate of mitochondrial respiration decreased following loss of p53 activity, and such transformed cells acquire a growth advantage. Oncogenic Ras increases

[1]Department of Molecular Oncology, Institute of Gerontology, Nippon Medical School, Kosugi-cho 1-396, Nakahara-ku, Kawasaki-shi, Kanagawa 211-8533, Japan.
[2]Correspondence should be addressed to N.T. (e-mail: nobuta@nms.ac.jp)

Received 31 December 2007; accepted 7 March 2008; published online 6 April 2008; DOI: 10.1038/ncb1724

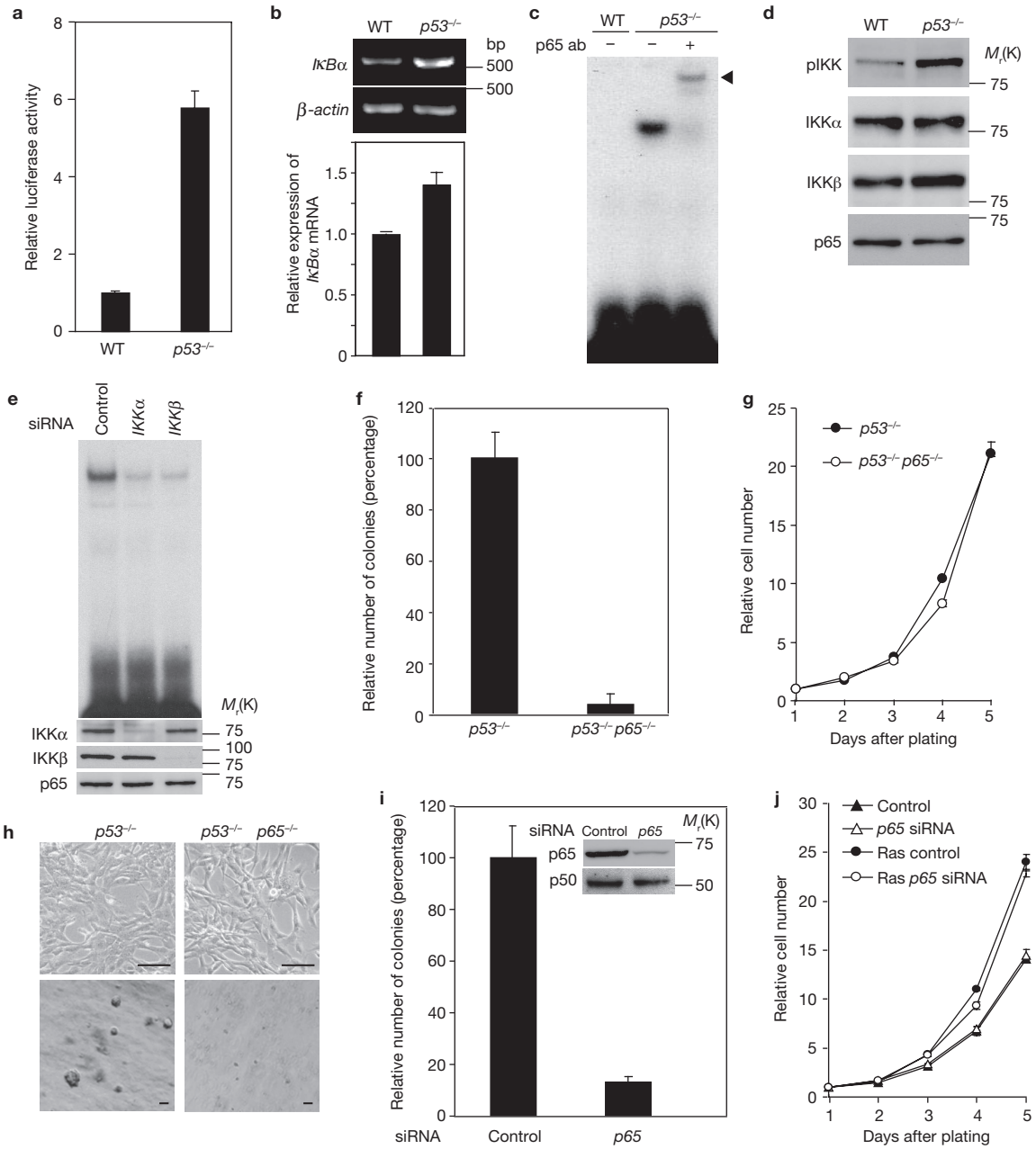

Figure 1 p65/NF-κB is important for Ha–RasV12-induced transformation of *p53*$^{-/-}$MEFs. (**a**) Wild-type (WT) and *p53*$^{-/-}$MEFs were cotransfected with the NF-κB Luc reporter plasmid and phRL-TK (internal control). After 24 h of transfection, relative luciferase activity was evaluated. (**b**) The expression of *IκBα*, a typical NF-κB target gene, in wild-type and *p53*$^{-/-}$ MEFs was examined by RT-PCR (top panel) or quantitative real-time PCR (bottom panel). (**c**) NF-κB DNA-binding activity in wild-type and *p53*$^{-/-}$MEFs was determined by EMSA. An anti-p65 antibody was mixed with the nuclear extracts of *p53*$^{-/-}$MEFs. Supershift bands are indicated by an arrowhead. (**d**) Phosphorylation of IKKα/β in wild-type and *p53*$^{-/-}$MEFs was determined by immunoblot analysis with an anti-phospho-IKK (pIKK) antibody. Representative data from several littermates are shown. (**e**) *p53*$^{-/-}$MEFs were infected with control-, *IKKα*- or *IKKβ*-siRNA-expressing retroviruses. NF-κB DNA-binding activity was determined by EMSA (top panel). The expression levels of IKKα and IKKβ were determined by immunoblot analysis (bottom panel). (**f**–**h**) *p53*$^{-/-}$ and *p53*$^{-/-}$*p65*$^{-/-}$MEFs were infected with Ha–RasV12-expressing retrovirus. MEFs were subjected to colony formation assays (**f**) and proliferation assays (**g**) over a 4-day period. (**h**) Morphological transformation (top panel) and colony formation in the soft agar (bottom panel) were observed. Scale bar, 100 μm. (**i**, **j**) *p53*$^{-/-}$MEFs were infected with control- or *p65*-siRNA-expressing retroviruses together with a Ha–RasV12-expressing retrovirus. Colony formation assays (**i**) and proliferation assays (**j**) were performed. (**i**) The expression level of p65 was determined by immunoblot analysis. Data are mean ± s. d. from three independent experiments (**a**, **b**, **f**, **g**, **i**, **j**). Uncropped images of the scans in **b** and **d** are shown in Supplementary Information, Fig. S7.

the rate of aerobic glycolysis by inducing the expression of glycolysis-regulating genes for cell transformation[3]. Although Ras is known to require NF-κB activation for cell transformation[12,21], little is known about the role of NF-κB in glycolysis. As shown in Fig. 2a, glucose consumption was increased in *p53*$^{-/-}$MEFs and reduced by p65 deficiency; however, glucose consumption in *p53*$^{-/-}$*p65*$^{-/-}$MEFs was still higher than that in wild-type MEFs. This suggests that p53 downregulates glycolysis-regulating factors in an NF-κB-dependent and independent manner. Glucose

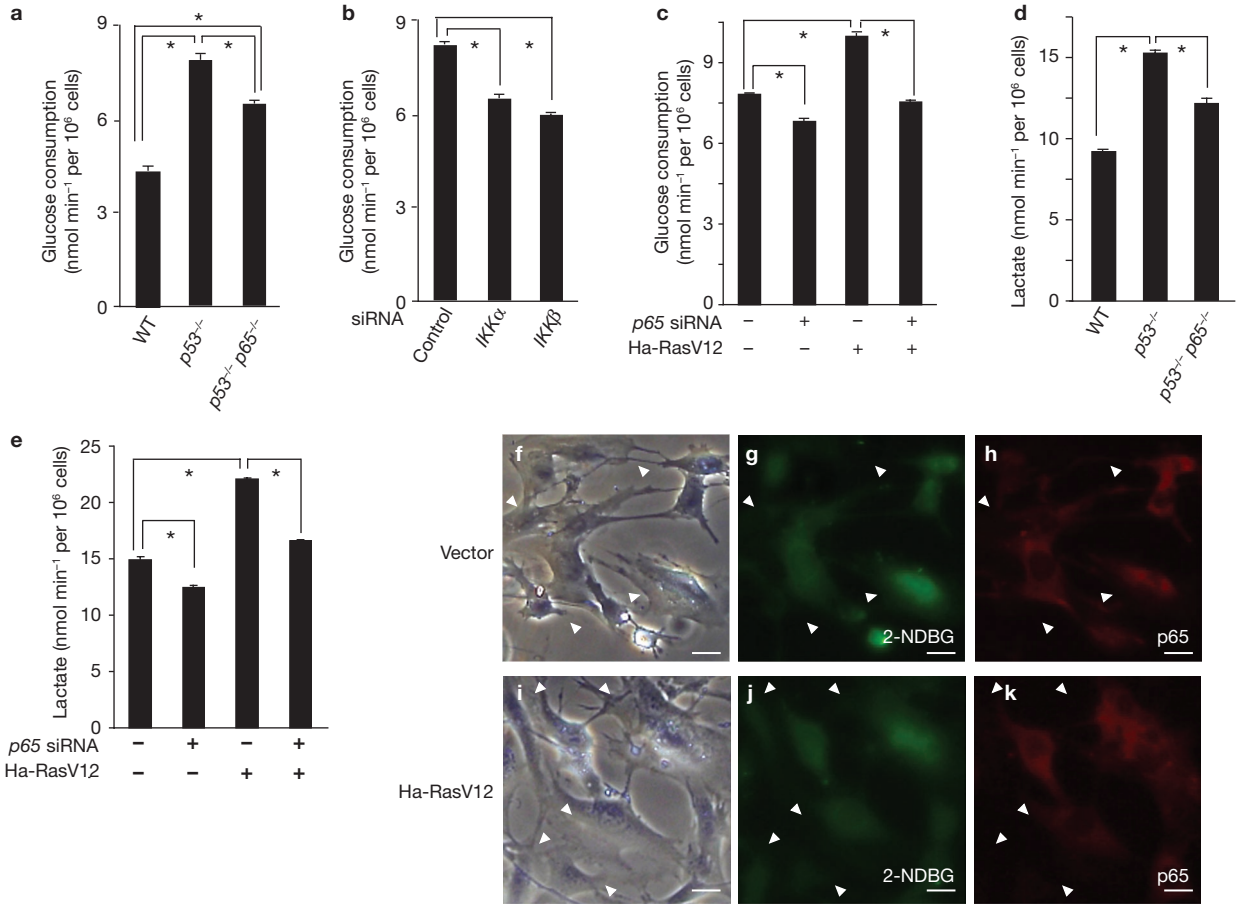

Figure 2 NF-κB is required for optimal aerobic glycolysis in $p53^{-/-}$MEFs. Glucose consumption (**a**) and lactate production (**d**) in wild-type, $p53^{-/-}$, and $p53^{-/-}p65^{-/-}$MEFs were measured. (**b**) $p53^{-/-}$MEFs were infected with control-, *IKKα*- or *IKKβ*-siRNA-expressing retroviruses and glucose consumption was measured. (**c**, **e**) $p53^{-/-}$MEFs were infected with the indicated retroviruses. Glucose consumption (**c**) and lactate production (**e**) were measured. Data are mean ± s. d. from three independent experiments (**a**–**e**). $*P < 0.01$ for indicated comparison (*t*-test). (**f**–**h**) $p53^{-/-}$MEFs were infected with control- or *p65*-siRNA-expressing retrovirus. (**i**–**k**) $p53^{-/-}$MEFs were infected with control- or *p65*-siRNA-expressing retroviruses together with a Ha–RasV12-expressing retrovirus. *p65* knockdown and control cells were seeded in the same glass-bottomed dish for analysis under closely comparable experimental conditions. Phase-contrast (**f**, **i**) and fluorescence imaging (**g**, **j**) of 2-NDBG (green) and immunocytochemistry for p65 (red; **h**, **k**). Arrowheads indicate cells with low levels of p65. Scale bar, 20 μm.

consumption of $p53^{-/-}p65^{-/-}$MEFs was increased by the re-introduction of wild-type p65 but not p65 S276A mutant[22], which is unable to activate transcription of multiple NF-κB-responsive genes (Supplementary Information, Fig. S1a, b). Furthermore, it was shown that glucose consumption in $p53^{-/-}$MEFs was decreased by knockdown of either *IKKα*, *IKKβ* (Fig. 2b) or *p65* (Fig. 2c). We found that glucose consumption of $p53^{-/-}$MEFs was further increased by introduction of Ha–RasV12 and decreased by *p65* knockdown (Fig. 2c). A high rate of glucose conversion to lactate is associated with a high rate of glucose uptake in the presence of oxygen, a metabolic change widely observed in cancer cells[1–4]. As expected, the observed changes in glucose consumption were associated with changes in lactate production (Fig. 2d, e). Oxygen consumption in $p53^{-/-}$MEFs was lower than that of wild-type MEFs, as previously reported[20], but was comparable to that of $p53^{-/-}p65^{-/-}$MEFs (Supplementary Information, Fig. S2a). In both $p53^{-/-}$MEFs and Ha–RasV12-expressing $p53^{-/-}$MEFs, knockdown of *p65* had little effect on oxygen consumption (Supplementary Information, Fig. S2b). These results indicate that in $p53^{-/-}$MEFs, p65 enhances glycolysis without affecting mitochondrial respiration. Taken together, these results show that enhanced activation of IKK–NF-κB, induced by the loss of p53 activity, has a crucial role in aerobic glycolysis. We next examined the effects of NF-κB on glucose uptake and showed that knockdown of *p65* in both $p53^{-/-}$MEFs (Fig. 2f–h) and Ha–RasV12-expressing $p53^{-/-}$MEFs (Fig. 2i–k) significantly decreased uptake of glucose, as seen by 2-NBDG uptake, a fluorescent analogue of D-glucose.

Uptake of glucose is mediated by the GLUT family, specifically, GLUT1 and GLUT3, both high-affinity glucose transporters. The expression of *GLUT1* and *GLUT3* appears to contribute to glycolysis in several human cancer cell lines[5,23,24]. We found that *Glut3* expression in $p53^{-/-}$MEFs was increased when compared with that of wild-type MEFs, but was decreased by p65 deficiency (Fig. 3a). Although it has been reported that p53 downregulates *Glut1* and *Glut4*[19], we found that expression of *Glut1* was comparable between wild-type and $p53^{-/-}$MEFs (Fig. 3a), whereas expression of *Glut4* was undetectable in $p53^{-/-}$MEFs (data not shown). *Glut3* expression in $p53^{-/-}$MEFs was clearly reduced by knockdown of either *IKKα*, *IKKβ* or *p65* (Fig. 3b, c). Re-introduction of wild-type p65, but not the p65 S276A mutant, to $p53^{-/-}p65^{-/-}$MEFs led to recovery of *Glut3* expression (Supplementary Information, Fig. S1c). We found that

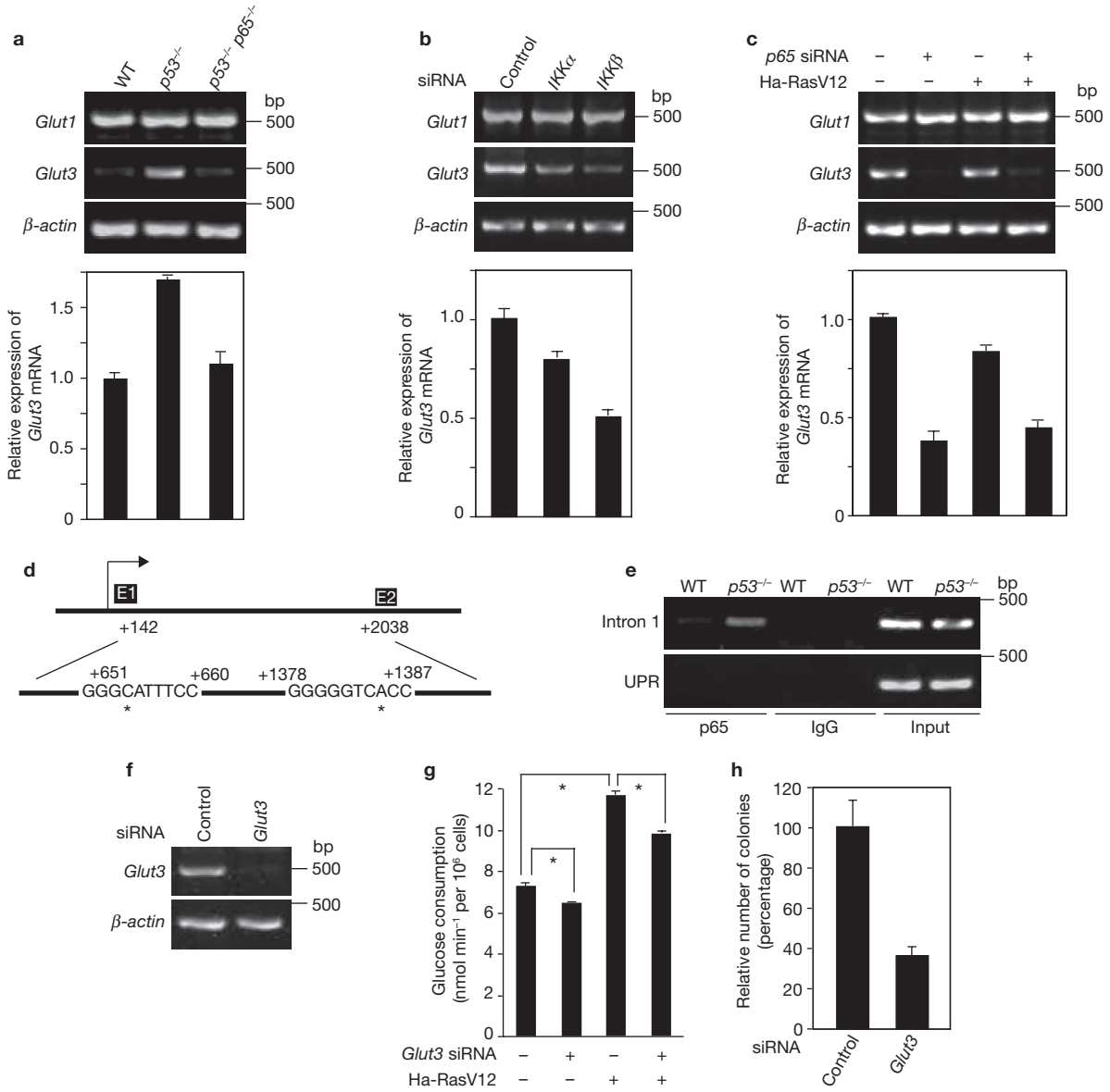

Figure 3 GLUT3 expression in *p53*$^{-/-}$MEFs is regulated by p65/NF-κB. (**a**–**c**) RT-PCR (top panels) and quantitative real-time PCR (bottom panels) were performed to examine *Glut1* and *Glut3* gene expression in wild-type, *p53*$^{-/-}$ and *p53*$^{-/-}$*p65*$^{-/-}$MEFs (**a**), *p53*$^{-/-}$MEFs infected with control-, *IKKα*- or *IKKβ*-siRNA-expressing retroviruses(**b**) and *p53*$^{-/-}$MEFs infected with the indicated retroviruses (**c**). (**d**) Two potential NF-κB binding sequences are located in intron 1 of the mouse *Glut3* gene. The site difference from the consensus NF-κB binding sequences (CBS) are indicated by asterisks. CBS, GGGRNNYYCC or HGGARNYYCC; R, purine; Y, pyrimidine; H indicates A, C or T. (**e**) Wild-type and *p53*$^{-/-}$MEFs were subjected to ChIP assay using an anti-p65 antibody. PCR amplifications were performed using primers surrounding the putative NF-κB binding site in intron 1 (position +351 to +699) or the upstream promoter region (UPR; position −1997 to −1687) lacking potential NF-κB binding site of the mouse *Glut3* gene. (**f**) *Glut3* expression in *p53*$^{-/-}$MEFs infected with control- or *Glut3*-siRNA-expressing retroviruses determined by RT-PCR. (**g**) Glucose consumption in *p53*$^{-/-}$MEFs infected with control or *Glut3* siRNA-expressing retroviruses, with or without a Ha–RasV12-expressing retrovirus. *$P < 0.01$ for indicated comparison (*t*-test). (**h**) The number of colonies formed in soft agar by *p53*$^{-/-}$MEFs infected with control- or *Glut3*-siRNA-expressing retroviruses together with a Ha–RasV12-expressing retrovirus. Data are mean ± s. d. from three independent experiments (**a**, **b**, **c**, **g**, **h**). Uncropped images of the scans in **a**, **b**, **c** and **e** are shown in Supplementary Information, Fig. S7.

two potential NF-κB binding sequences were encompassed within intron 1 of the mouse *Glut3* gene, and one of them responded to p65 (Fig. 3d; Supplementary Information, Fig. S1d, e). Furthermore, it was implied by chromatin immunoprecipitation (ChIP) analysis that p65 binds to the predicted site in *p53*$^{-/-}$MEFs (Fig. 3e), suggesting that GLUT3 expression is directly regulated by NF-κB. We next examined whether enhanced glycolysis in *p53*$^{-/-}$MEFs is caused by NF-κB-induced *Glut3* expression. In *p53*$^{-/-}$MEFs, knockdown of *Glut3* decreased glucose consumption and suppressed Ha–RasV12-induced anchorage-independent colony formation (Fig. 3f–h). Although glucose consumption was further increased by introduction of Ha–RasV12 to *p53*$^{-/-}$MEFs (Figs 2c, 3g), expression of *Glut3* was not elevated by Ha–RasV12 expression in *p53*$^{-/-}$MEFs (Fig. 3c). It remains unclear why *Glut3* expression in *p53*$^{-/-}$MEFs is not enhanced by Ras; however, enhanced expression of *Glut3* by p53-deficiency-induced NF-κB activation may be critical for the maintenance of Ras-dependent acceleration of glycolysis and so support transformation. Furthermore,

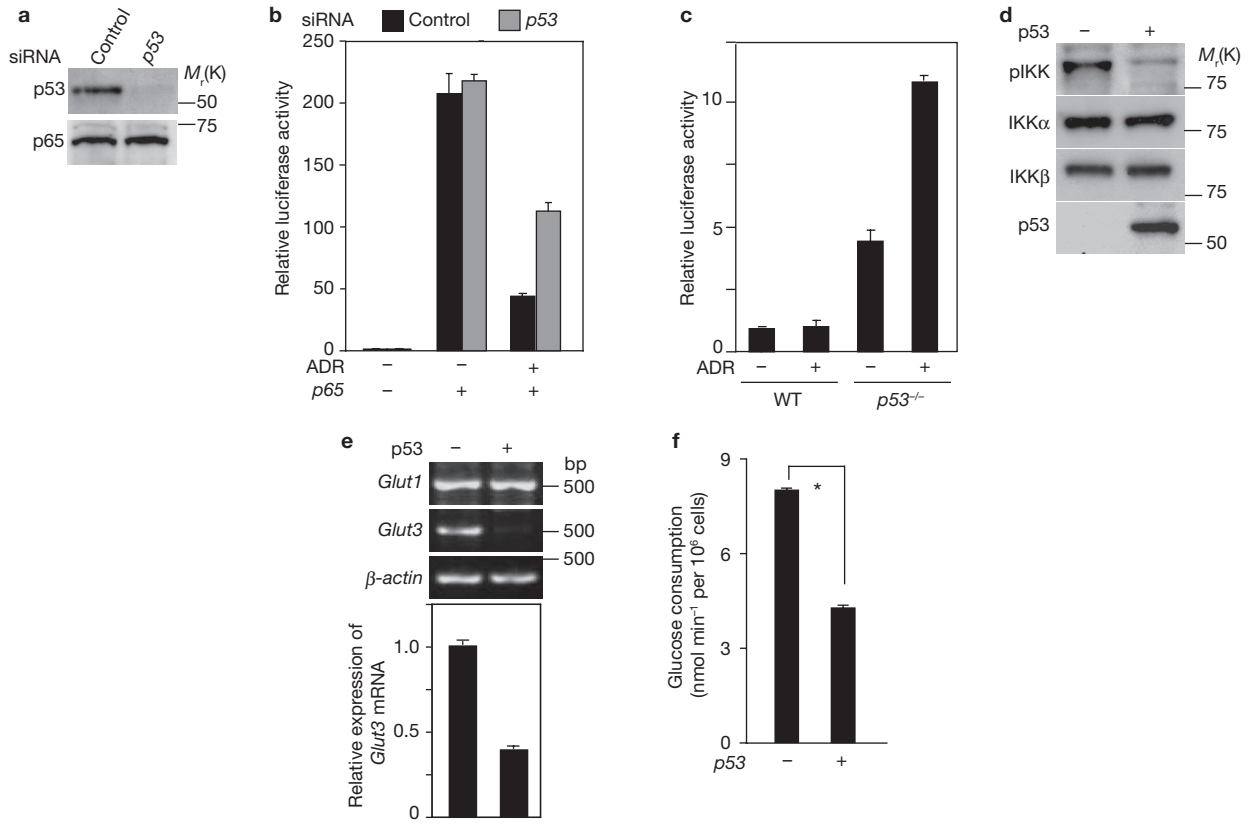

Figure 4 Activated p53 suppresses NF-κB activity and aerobic glycolysis. (**a**, **b**) MCF-7 cells were infected with control- or *p53*-siRNA-expressing retroviruses. The expression level of p53 was determined by immunoblot analysis (**a**). Cells were cotransfected with the NF-κB Luc reporter plasmid, the p65 expression vector and phRL-TK. After 12 h from transfection, transfected cells were treated with adriamycin (ADR, 0.5 μg ml^{-1}) for 24 h and relative luciferase activity was evaluated (**b**). (**c**) Wild-type and *p53*$^{-/-}$ MEFs were transfected with the NF-κB Luc reporter plasmid and phRL-TK. After 12 h of transfection, cells were treated with or without adriamycin for 24 h and relative luciferase activity was evaluated. (**d**) Lysates from the *p53*$^{-/-}$MEFs infected with p53-expressing retroviruses were subjected to immunoblot analysis with the indicated antibodies. (**e**, **f**) *Glut1* or *Glut3* gene expression examined by RT-PCR (**e**, top panel) or quantitative real-time PCR (**e**, bottom panel) and glucose consumption (**f**) in *p53*$^{-/-}$MEFs were infected with p53-expressing retroviruses. $^*P < 0.01$ for indicated comparison (*t*-test). Data are mean ± s. d. from three independent experiments (**b**, **c**, **e**, **f**). Uncropped images of the scans in **d** and **e** are shown in Supplementary Information, Fig. S7.

both glucose consumption (Figs 2c, 3g) and anchorage-independent colony formation (Figs 1i, 3h) were more effectively suppressed by *p65* knockdown than by *Glut3* knockdown, suggesting that other target(s) of NF-κB also regulate these processes. Therefore, it is conceivable that glycolysis-regulating factors including GLUT3 and other NF-κB targets such as anti-apoptotic factors and cell adhesion molecules[25], in combination, promote Ha–RasV12-induced transformation.

In unstimulated conditions p53 was unstable, but was stabilized by genotoxic stress, as has been shown previously[7] (Supplementary Information, Fig. S3a, b). In normal cells, activation of p53, following induction of the DNA-damage response by oncogenes, causes apoptosis or senescence, which prevent transformation[10,11]. We next examined whether these effects of activated p53 involve suppression of NF-κB activation. It was shown that p65-dependent transcriptional activity was suppressed by adriamycin-induced DNA damage; activated p53 participated in this suppression as it was attenuated by *p53* knockdown (Fig. 4a, b) and in *p53*$^{-/-}$MEFs adriamycin enhanced NF-κB transcriptional activity (Fig. 4c). IKKα and IKKβ were activated by DNA damage, as described previously[17]; however, 24 h after treatment with adriamycin, the activities of these kinases had been suppressed in wild-type MEFs but were sustained in *p53*$^{-/-}$MEFs (Supplementary Information, Fig. S3a, b). We therefore examined whether activated p53 suppresses the activity of IKKα and IKKβ and found that ectopically expressed p53 could suppress endogenous and exogenous IKK activity in *p53*$^{-/-}$MEFs (Fig. 4d; Supplementary Information, Fig. S3c). Of note, the DNA-binding activity of NF-κB was sustained for up to 24 h after treatment with adriamycin in both wild-type and *p53*$^{-/-}$MEFs (Supplementary Information, Fig. S3d). Sustained activation of IKKα and IKKβ induced by adriamycin in *p53*$^{-/-}$MEFs may induce both DNA-binding activity (Supplementary Information, Fig. S3d, lanes 5, 8) and the transcriptional activity of NF-κB (Fig. 4c). In wild-type MEFs, the DNA-binding activity of NF-κB remained elevated 24 h after treatment with adriamycin, in spite of low IKK activity (Supplementary Information, Fig. S3d, lanes 1, 4); however, we assumed that NF-κB was in a transcriptionally inactivated state (Fig. 4c). We considered the possibility that activated p53 induces DNA binding of NF-κB but suppresses transcriptional activity of NF-κB at the promoter in wild-type MEFs. We therefore characterized transcriptional complexes at the typical NF-κB target gene, *IκBα* promoter, using ChIP assays (Supplementary Information, Fig. S3e). As previously reported[26,27], IKKα was recruited to the *IκBα* promoter in wild-type MEFs. In *p53*$^{-/-}$MEFs, the recruitment of p65, IKKα and phosphorylated histone H3 to the promoter was enhanced. As IKKα catalyses phosphorylation of histone H3, which is a key modulator of NF-κB transcriptional activity[26,27],

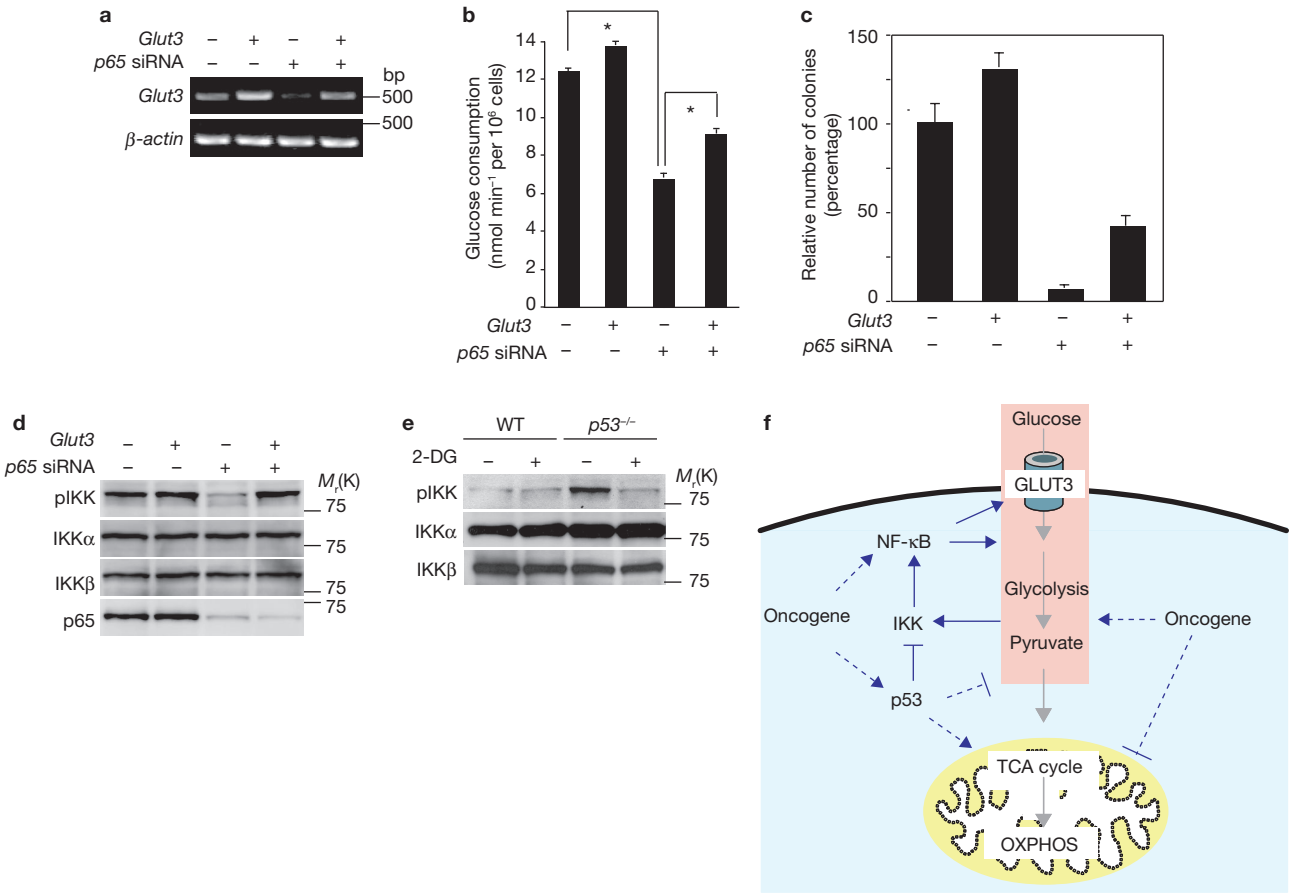

Figure 5 Glycolysis drives IKK activation in *p53*$^{-/-}$MEFs. (**a**–**d**) Ha-RasV12-expressing *p53*$^{-/-}$MEFs infected with control- or *p65*-siRNA-expressing retroviruses were superinfected with the control vector or GLUT3-expressing retrovirus. *Glut3* gene expression was examined by RT-PCR (**a**), glucose consumption was measured (**b**; $*P < 0.01$ for indicated comparison using *t*-test) and the number of colonies formed in soft agar were counted (**c**). Data are mean ± s. d. from three independent experiments (**b**, **c**). (**d**) Phosphorylation of IKKα/β was determined by immunoblot analysis. (**e**) Wild-type and *p53*$^{-/-}$MEFs were treated with 2-DG (2-deoxy-D-glucose; 4.5 mg ml^{-1}) for 2 h. Phosphorylation of IKKα/β was determined by immunoblot analysis. (**f**) Model of the proposed link between p53, NF-κB and glycolysis. The blue solid lines indicate our model in which p53 regulates an activation loop in IKK, NF-κB and the glucose metabolism. The blue broken lines indicate previously reported regulation. OXPHOS; oxidative phosphorylation. Uncropped images of the scans in **d** and **e** are shown in Supplementary Information, Fig. S7.

enhanced recruitment of p65 and phosphorylated histone H3 may be attributed to the enhanced activity of IKKα and/or IKKβ, induced by loss of p53 activity in *p53*$^{-/-}$MEFs. Similarly, after stimulation with adriamycin for 24 h, recruitment of p65, IKKβ and phosphorylated histone H3 to the promoter was enhanced in *p53*$^{-/-}$MEFs. In wild-type MEFs, recruitment of p53 was observed and phosphorylated histone H3 was clearly decreased by adriamycin. In contrast to *p53*$^{-/-}$MEFs, endogenous IKKs were not activated in the unstimulated condition or after stimulation with adriamycin for 24 h in wild-type MEFs (Supplementary Information, Fig. S3a, b). These results suggest that activated p53 inhibits the phosphorylation of histone H3 by suppression of another histone H3 kinase(s), in addition to IKKα. Although it remains unclear why enhanced recruitment of IKKα and adriamycin-induced recruitment of IKKβ were observed in *p53*$^{-/-}$MEFs, IKKβ may contribute to the phosphorylation of histone H3 in response to adriamycin through activation of IKKα.

We next examined whether activation of p53 causes downregulation of *Glut3* expression, and found that re-introduction of p53 to *p53*$^{-/-}$MEFs suppressed *Glut3* expression and glucose consumption in these cells (Fig. 4e, f). In agreement with reports that suggest cancer-associated p53 mutants induce NF-κB activation[28], the transcriptional activity of NF-κB was induced by expression of three p53 mutants: R175H, R248W and R273H in wild-type MEFs and NIH3T3 cells (Supplementary Information, Fig. S4a). In wild-type MEFs, the p53 R175H mutant enhanced IKK activity (Supplementary Information, Fig. S4b), suggesting that activation of IKK is restricted by wild-type p53. Cell transformation of Ha–RasV12-expressing wild-type MEFs induced by the p53 R175H mutant was suppressed by *p65* knockdown (Supplementary Information, Fig. S4c). Under these conditions, glucose consumption and expression of *Glut3*, which were enhanced by p53 R175H, were also decreased by *p65* knockdown (Supplementary Information, Fig. S4d, e). These results suggest that enhanced activation of NF-κB, induced by the p53 mutant, has an important role in oncogene-induced cell transformation and acceleration of glycolysis in wild-type MEFs.

Colony formation of Ha–RasV12-expressing *p53*$^{-/-}$MEFs was further increased by exogenous *Glut3* expression (Fig. 5a, c); however, exogenous *Glut3* by itself was unable to induce this transformation (data not shown) in spite of the increased glucose consumption by *p53*$^{-/-}$MEFs (*see* Supplementary Information, Fig. S5a, b). We next examined whether

exogenous expression of *Glut3* was able to restore colony formation in $p53^{-/-}$MEFs with *p65* knockdown and in $p53^{-/-}p65^{-/-}$MEFs. We found that *Glut3* expression partially restored Ha–RasV12-induced colony formation and glucose consumption in both $p53^{-/-}$MEFs with *p65* knockdown (Fig. 5a–c) and in $p53^{-/-}p65^{-/-}$MEFs (Supplementary Information, Fig. S6a–c). These results indicate that G*lut3* did not act as an oncogene, but that the enhanced GLUT3-mediated uptake of glucose accelerates cell transformation in Ha–RasV12-expressing $p53^{-/-}$MEFs through an NF-κB-independent pathway.

Interestingly, we found that the hyperactivation of IKK in Ha–RasV12-expressing $p53^{-/-}$MEFs was suppressed by knockdown or deficiency of p65, and that this was restored by exogenously expressed *Glut3* (Fig. 5d; Supplementary Information, Fig. S6d). Additionally, the glycolytic inhibitor 2-deoxy-D-glucose (2-DG) decreased the enhanced activation of IKK in $p53^{-/-}$MEFs (Fig. 5e). Exogenous expression of *Glut3* led to increased glucose consumption in both wild-type and $p53^{-/-}$MEFs, but enhanced IKK activation was only observed in $p53^{-/-}$MEFs (Supplementary Information, Fig. S5c). These results suggest that acceleration of glycolysis drives a positive-feedback loop in the IKK–NF-κB pathway, which is induced by p53 deficiency.

A model for the proposed link between p53, NF-κB and glycolysis is shown in Fig 5f. p53 restricts IKK–NF-κB activation and subsequently suppresses glycolysis through downregulation of NF-κB-dependent genes (including *Glut3*), downregulation of PGM[18] and upregulation of TIGAR (TPp53-induced glycolysis and apoptosis regulator)[29], and increases mitochondrial respiration through upregulation of SCO2[20]. When p53 function is lost, oncogene expression increases the rate of glycolysis and decreases the rate of mitochondrial respiration — the Warburg effect — in transformed cells. So how does p53 suppress the kinase activities of IKKα and IKKβ? Although it is possible that IKKs activities are directly suppressed by a p53 target gene(s), an alternative explanation is that p53 restricts the activation of the IKK–NF-κB pathway through suppression of aerobic glycolysis.

In summary, both basally expressing p53 and genotoxic stress-activated p53 inhibits the kinase activities of IKKα and IKKβ and the transcriptional activity of NF-κB. Deficiency of p53 enhances NF-κB-dependent glucose metabolism, which is partially depend on GLUT3. Moreover, in cells that evade a p53-mediated tumour surveillance system, oncogene-induced cell transformation requires NF-κB activation. Therefore, the positive-feedback loop by which glycolysis drives IKK–NF-κB activation may have an important role in oncogenesis.

METHODS

Cell culture and retroviral infection. Cells were cultured in Dulbecco's modified Eagle's medium supplemented with 10% fetal bovine serum (FBS) and 50 μg ml^{-1} kanamycin. Retroviral infection was performed as described previously[30]. Infected cells were selected using puromycin (1 μg ml^{-1}), hygromycin (200 μg ml^{-1}), zeocin (500 μg ml^{-1}) or blastidin (2.5 μg ml^{-1}).

Mice. $p53^{-/-}$ mice were purchased from Taconic and $p65^{-/-}$mice from the Riken Bio Resource Center. Animal experiments were reviewed by the Ethics Committee on Animal Experiments of Nippon Medical School and were carried out in accordance with the guidelines for Animal Experiments of Nippon Medical School and the guidelines of The Law and Notification of the government of Japan. MEFs were prepared as described previously[30].

Plasmids. pNF-κB Luc was obtained from Clontech Laboratories. pGLUT3+651 Luc or pGLUT3+1378 Luc were replaced by the NF-κB response element of pNF-κB Luc to (+651 GGGCATTTCC × 4) or (+1378 GGGGGTCACC × 4). The control plasmid phRL-TK (renila luciferase reporter) was obtained from Toyobo. pEF-p53 R175H, R248W and R273H are mutants in which Arg 175, 248 or 273 of p53 are replaced by His or Trp. Full-length human *p65* cDNA was obtained by PCR from HeLa cDNA pools and cloned into a pcDNA3-Flag vector. pcDNA3-Flag-p65 S276A, in which Ser 276 of p65 is replaced by Ala, was then generated. Retroviral vectors of pBabe Ha–RasV12 with selection markers for puromycin or hygromycin were used. Full-length mouse *Glut3* cDNA was obtained by PCR from an NIH3T3 cDNA pool, and cloned into the pBabe blast vector. A retroviral vector for pBabe p53 with a selection marker for puromycin or a vector for pBabe p53 R175H with a selection marker for zeocin was used.

RNA interference. The retroviral vectors pSuper-shp65 puro, -shIKKα puro, -shIKKβ puro and -shGLUT3 puro were cloned with mouse *p65* target sequence GAAGAAGAGTCCTTTCAAT, mouse *IKKα* target sequence GCAATTAAGTCTTGTCGTT, mouse *IKKβ* target sequence GGACATCGTTGTTAGTGAA, mouse *GLUT3* target sequence CAACAGGAATCTTCAAGGA, respectively, into a pSuper puro vector (Oligoengine).

Antibodies and materials. Anti-HA (Covance) antibody was used for immunoprecipitation. Anti-p53 polyclonal (1:1000, FL393; Santa Cruz Biotechnology), anti-p53 monoclonal (1:500, Ab-5; Neo Marker), anti-IKKα monoclonal (1:500; Oncogene Research Product), anti-IKKβ monoclonal (1:500; Cell Signaling Technology), anti-phospho-IKK (IKKα [Ser 180]/IKKβ [Ser 181], 1:500; Cell Signaling Technology) and anti-p65 polyclonal (1:100, sc-372; Santa Cruz Biotechnology) antibodies were used for immunoblot analysis. Adriamycin (0.5 μg ml^{-1}) was obtained from Calbiochem.

Electrophoretic mobility shift assay (EMSA). Cells were solubilized in buffer (10 mM HEPES pH 7.2, 10 mM KCl, 0.1 mM EDTA, 0.1 mM EGTA, 0.4% NP-40, protease inhibitor cocktail, 1 mM DTT) and centrifuged at 10,000*g* for 10 min. Pellets were resuspended in buffer (20 mM HEPES pH 7.9, 400 mM NaCl, 1 mM EDTA, 1 mM EGTA, protease inhibitor cocktail (Nakarai Tesque), 1 mM DTT) and then centrifuged at 20,000*g* for 15 min. The supernatant was used as the nuclear extract. ^{32}P-labelled DNA probes to the NF-κB binding site (underlined), AGCTTCAGAGGGGACTTTCCGAGAGG were prepared. Nuclear extracts (10 μg of protein) were incubated with the ^{32}P-labelled probes (100,000 cpm) in 20 μl of buffer (20 mM HEPES pH 7.9, 5% glycerol, 1 mM EDTA, 100 μg ml^{-1} poly dI-dC) for 20 min at room temperature. Samples were subjected to 5% polyacrylamide gel electrophoresis.

RT-PCR and quantitative real-time PCR. Total RNA was extracted using a DNA-free kit (Qiagen) and purified using an RNeasy kit (Qiagen). cDNA was prepared using oligonucleotide (dT), random primers and Superscript III (Invitrogen). RT-PCR analysis of *IκBα*, *Glut1*, *Glut3* or *β-actin* as a control was carried out using the following primer pairs: *IκBα* 499 bp, 5′-ATGTTTCAGCCAGCTGGGCAC-3′ forward and 5′-AGGTCTGCGTCAAGACTGCTAC-3′ reverse; *Glut1* 504 bp, 5′-ATGGATCCCAGCAGCAAGAAGGTGACGGGC -3′ forward and 5′- GATGCCAACGACGATTCCCAGCT-3′ reverse; *Glut3* 509 bp, 5′-ATGGGGACAACGAAGGTGACCCCATCTCTG-3′ forward and 5′-TGAGCTACCAGAATCCCAACAACG-3' reverse, *β-actin* 313 bp, 5′-ATGGATGACGATATCGCTGCGC-3′ forward and 5′-GCAGCACAGGGTGCTCCTCA-3′ reverse. Quantitative real-time PCR analysis was performed using a TaqMan Probe Mix (Applied Biosystems) under the following conditions: 15 min at 95°C followed by 40 cycles of 95°C for 15 s and 60°C for 1 min, using an ABI Prism 7700 sequence detection system. The primer and probe sets used were: mouse *IκBα* forward, 5′-GCGGGATGGCCTCAAGA-3′, reverse 5′-TCTCCCGCAGCTCCTTCA-3′, probe, 5′-FAM-CATGAAGGACGAGGAGTA-NFQ-3′; predesigned primer/probe sets for mouse GLUT3, β-actin are commercially available (GLUT3, Mm00441483 m1, β-actin, Mm 00607939 s1), with all primers and probes synthesized. Data show mRNA expression levels relative to those of *β-actin*; the former was then normalized to control expression levels for each experiment.

Colony formation assay. A layer of 0.5% (wt/vol) agarose in normal medium was prepared in the six-well plates and a layer of 0.6% agarose containing 1×10^5 infected cells was poured over the first layer. The number of colonies that had formed in the soft agar was counted after two weeks.

Measurements of glucose consumption and lactate production. Cells were seeded in culture dishes and the medium changed after 6 h. Cells were incubated for 14–18 h and the culture medium was then collected for measurement of glucose and lactate concentrations. Glucose levels were determined using a Glucose (GO) assay kit (Sigma). Glucose consumption was determined from the difference in glucose concentration compared with control. Lactate levels were determined using an F-kit L-lactate (J. K. International).

Measurement of 2-NBDG uptake and immunocytochemistry. MEFs were plated in a glass-bottom dish and cultured overnight. MEFs were preincubated in glucose-free KRB buffer for 15 min at 37°C and cells incubated in fresh KRB buffer supplemented with 600 μM 2-NBDG (2-[*N*-(7-nitrobenz-2-oxa-1,3-diazol-4-yl)amino]-2-deoxyglucose; Molecular Probes) and 3.3 mM glucose for 10 min at 37°C. After washing with KRB buffer, MEFs were imaged at 488 nm using a fluorescence microscope (Keyence BZ-8000). After quantification of fluorescence, MEFs were fixed and immunostained for p65.

Note: Supplementary Information is available on the Nature Cell Biology website.

ACKNOWLEDGEMENTS

We thank T. Taniguchi, M. Oren, H. Hirata, K. Sada, S. Minami, S. Ohta, S. Asoh, O. Kawanami, I. Ohsawa, W. A. Martin, E. Oda-Sato, Y. Abe, W. Nakajima and M. Ando for discussion; T. Doi, S. Mise and Y. Asano for technical support; I. Uehara for preparation of MEFs; R. Agami for the retroviral vectors pSuper-sh human p53 puro; D. V. Goeddel for *IKKα* and *IKKβ* cDNA. This work was supported by Grants-in-aid from the Ministry of Education, Culture, Sports, Science and Technology of Japan.

AUTHOR CONTRIBUTIONS

K. K. and N. T. designed the study; K. K., with contributions from K. A. and K. T., performed all experiments; K. K. and N. T. wrote the manuscript.

Published online at http://www.nature.com/naturecellbiology/
Reprints and permissions information is available online at http://npg.nature.com/reprintsandpermissions/

1. Warburg, O. On respiratory impairment in cancer cells. *Science* **124,** 269–270 (1956).
2. Kim, J. W. & Dang, C. V. Cancer's molecular sweet tooth and the Warburg effect. *Cancer Res.* **66,** 8927–8930 (2006).
3. Dang, C. V. & Semenza, G. L. Oncogenic alterations of metabolism. *Trends Biochem. Sci.* **24,** 68–72 (1999).
4. Gatenby, R. A. & Gillies, R. J. Why do cancers have high aerobic glycolysis? *Nature Rev. Cancer* **4,** 891–899 (2004).
5. Meller, J., Sahlmann, C. O. & Scheel, A. K. 18F-FDG PET and PET/CT in fever of unknown origin. *J. Nucl. Med.* **48,** 35–45 (2007).
6. Hamroun, D. *et al.* The UMD TP53 database and website: update and revisions. *Hum. Mutat.* **27,** 14–20 (2006).
7. Vogelstein, B., Lane, D. & Levine, A. J. Surfing the p53 network. *Nature* **408,** 307–310 (2000).
8. Lowe, S. W., Jacks, T., Housman, D. E. & Ruley, H. E. Abrogation of oncogene-associated apoptosis allows transformation of p53-deficient cells. *Proc. Natl Acad. Sci. USA* **91,** 2026–2030 (1994).
9. Tanaka, N. *et al.* Cellular commitment to oncogene-induced transformation or apoptosis is dependent on the transcription factor IRF-1. *Cell* **77,** 829–839 (1994).
10. Bartek, J., Lukas, J. & Bartkova, J. DNA damage response as an anti-cancer barrier: damage threshold and the concept of 'conditional haploinsufficiency'. *Cell Cycle* **6,** 2344–2347 (2007).
11. Serrano, M., Lin, A. W., McCurrach, M. E., Beach, D. & Lowe, S. W. Oncogenic *ras* provokes premature cell senescence associated with accumulation of p53 and p16INK4a. *Cell* **88,** 593–602 (1997).
12. Finco, T. S. *et al.* Oncogenic Ha-Ras-induced signaling activates NF-κB transcriptional activity, which is required for cellular transformation. *J. Biol. Chem.* **272,** 24113–24116 (1997).
13. Rayet, B. & Gelinas, C. Aberrant *rel/nfκb* genes and activity in human cancer. *Oncogene* **18,** 6938–6947 (1999).
14. Ryan, K. M., Ernst, M. K., Rice, N. R. & Vousden, K. H. Role of NF-κB in p53-mediated programmed cell death. *Nature* **404,** 892–897 (2000).
15. Webster, G. A. & Perkins, N. D. Transcriptional cross talk between NF-κB and p53. *Mol. Cell. Biol.* **19,** 3485–3495 (1999).
16. Huang, W. C., Ju, T. K., Hung, M. C. & Chen, C. C. Phosphorylation of CBP by IKKα promotes cell growth by switching the binding preference of CBP from p53 to NF-κB. *Mol. Cell* **26,** 75–87 (2007).
17. Janssens, S. & Tschopp, J. Signals from within: the DNA-damage-induced NF-κB response. *Cell Death Differ.* **13,** 773–784 (2006).
18. Kondoh, H. *et al.* Glycolytic enzymes can modulate cellular life span. *Cancer Res.* **65,** 177–185 (2005).
19. Schwartzenberg-Bar-Yoseph, F., Armoni, M. & Karnieli, E. The tumor suppressor p53 down-regulates glucose transporters GLUT1 and GLUT4 gene expression. *Cancer Res.* **64,** 2627–2633 (2004).
20. Matoba, S. *et al.* p53 regulates mitochondrial respiration. *Science* **312,** 1650–1653 (2006).
21. Mayo, M. W. & Baldwin, A. S. The transcription factor NF-κB: control of oncogenesis and cancer therapy resistance. *Biochim. Biophys. Acta* **1470**, M55-62 (2000).
22. Zhong, H., Voll, R. E. & Ghosh, S. Phosphorylation of NF-κB p65 by PKA stimulates transcriptional activity by promoting a novel bivalent interaction with the co-activator CBP/p300. *Mol. Cell* **1,** 661–671 (1998).
23. Macheda, M. L., Rogers, S. & Best, J. D. Molecular and cellular regulation of glucose transporter (GLUT) proteins in cancer. *J. Cell Physiol.* **202,** 654–662 (2005).
24. Medina, R. A. & Owen, G. I. Glucose transporters: expression, regulation and cancer. *Biol. Res.* **35,** 9–26 (2002).
25. Pahl, H. L. Activators and target genes of Rel/NF-κB transcription factors. *Oncogene* **18,** 6853–6866 (1999).
26. Anest, V. *et al.* A nucleosomal function for IκB kinase-α in NF-κB-dependent gene expression. *Nature* **423,** 659–663 (2003).
27. Yamamoto, Y., Verma, U. N., Prajapati, S., Kwak, Y. T. & Gaynor, R. B. Histone H3 phosphorylation by IKK-α is critical for cytokine-induced gene expression. *Nature* **423,** 655–659 (2003).
28. Weisz, L. *et al.* Mutant p53 enhances nuclear factor κB activation by tumor necrosis factor α in cancer cells. *Cancer Res.* **67,** 2396–2401 (2007).
29. Bensaad, K. *et al.* TIGAR, a p53-inducible regulator of glycolysis and apoptosis. *Cell* **126,** 107–120 (2006).
30. Sato, M. *et al.* Distinct and essential roles of transcription factors IRF-3 and IRF-7 in response to viruses for IFN-α/β gene induction. *Immunity* **13,** 539–548 (2000).

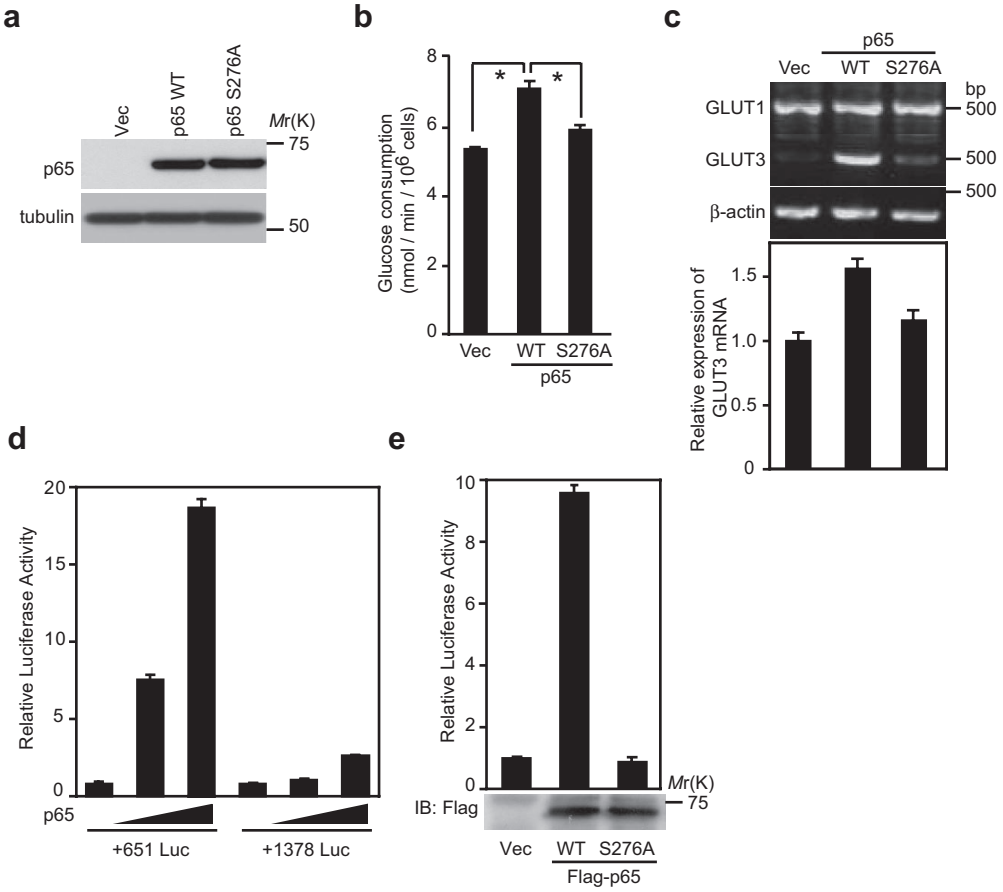

Figure S1 Enhanced glycolysis and *GLUT3* expression in *p53*$^{-/-}$ MEFs are dependent on NF-κB transcriptional activity. **(a-c)** *p53*$^{-/-}$*p65*$^{-/-}$MEFs were infected with wild-type-p65- or mutant-p65 (S276A)-expressing retroviruses. Lysates from the infected MEFs were subjected to immunoblot analysis **(a)**. Glucose consumption in the infected MEFs was measured **(b)**. *, $p < 0.01$ for indicated comparison (t-test). *GLUT1* or *GLUT3* gene expression was examined by RT-PCR (top panel), or quantitative real-time PCR (bottom panel) **(c)**. **(d)** NIH3T3 cells were cotransfected with the pGLUT3+651 Luc or pGLUT3+1378 Luc reporter plasmids and the p65 expression vector (20 or 200 ng) together with phRL-TK, as an internal control. **(e)** *p53*$^{-/-}$MEFs were cotransfected with the pGLUT3+651 Luc reporter plasmid and wild-type-p65 or mutant-p65 (S276A) expression vectors together with phRL-TK. After 24 h from transfection, relative luciferase activity was evaluated. Expression from these constructs was verified by immunoblot analysis. In b-e, data are mean ±s.d. from three independent experiments.

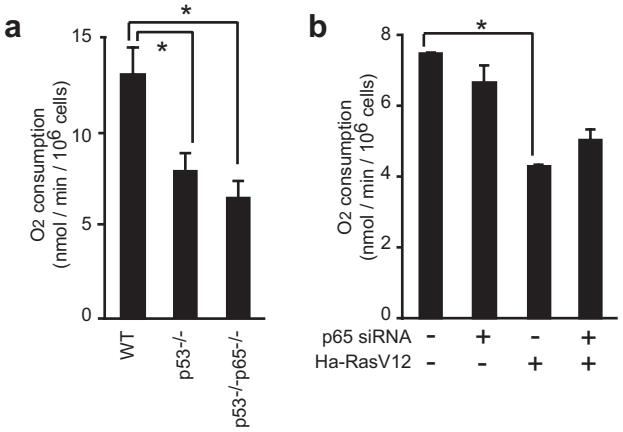

Figure S2 p65-deficiency does not affect oxygen consumption. **(a)** Oxygen consumption was measured in wild-type, *p53*$^{-/-}$, and *p53*$^{-/-}$*p65*$^{-/-}$MEFs. **(b)** *p53*$^{-/-}$MEFs were infected with control- or p65-siRNA, with or without a Ha-RasV12-expressing retrovirus. Oxygen consumption was measured. In a and b, data are mean ±s.d. from three independent experiments. *, $p < 0.01$ for indicated comparison (t-test).

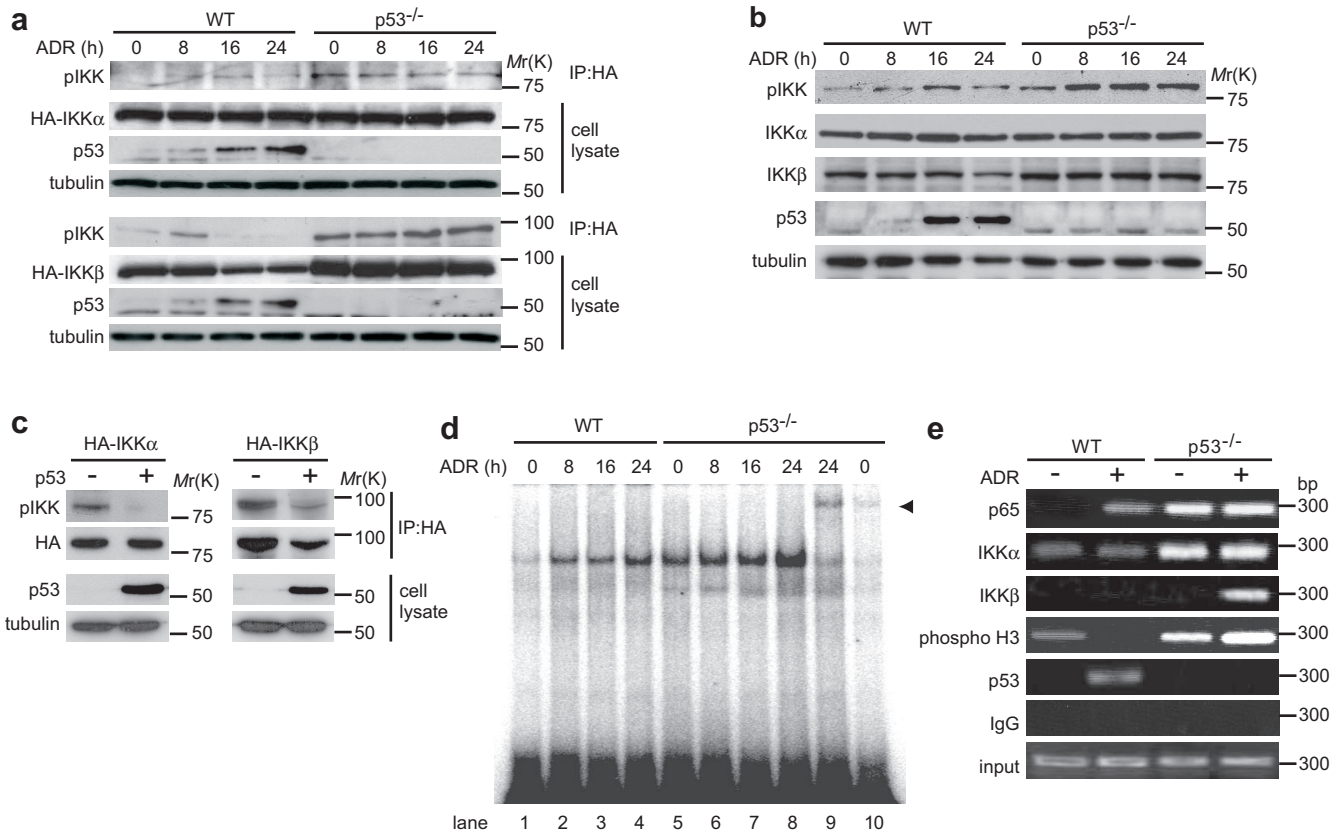

Figure S3 Activity of IKKα and IKKβ is suppressed by activated p53. **(a)** Wild-type and *p53*$^{-/-}$MEFs were transfected with HA-tagged IKKα (top panel) or HA-tagged IKKβ (bottom panel) and treated with adriamycin (0.5 μg ml^{-1}) for the indicated periods. Lysates from the transfected MEFs were subjected to immunoprecipitation with an anti-HA antibody and immunoblot analysis carried out with an anti-phospho-IKK (pIKK) antibody. Tubulin was used as a loading control. **(b)** Wild-type and *p53*$^{-/-}$MEFs were treated with adriamycin for the indicated periods. Cell lysates were subjected to immunoblot analysis with an anti-phospho-IKK (pIKK) antibody. **(c)** HA-tagged IKKα (left panel) or HA-tagged IKKβ (right panel) expression vectors were transfected into *p53*$^{-/-}$MEFs, with or without a p53 expression vector, and cell extracts prepared 24 h after transfection. IKK phosphorylation was evaluated by immunoprecipitation with an anti-HA antibody followed by immunoblot analysis with an anti-phospho-IKK (pIKK) antibody. **(d)** Wild-type and *p53*$^{-/-}$MEFs were treated with adriamycin for the indicated periods. Nuclear extracts were subjected to EMSA. p65 antibody was mixed with nuclear extracts (lanes 9 and 10). Supershift bands are indicated by an arrowhead. **(e)** The bindings of p65, IKKα, IKKβ, p53, and phospho-histone H3 (phospho H3) to the *IκBα* promoter were examined by ChIP assay using wild-type and *p53*$^{-/-}$MEFs treated with adriamycin for 24 h.

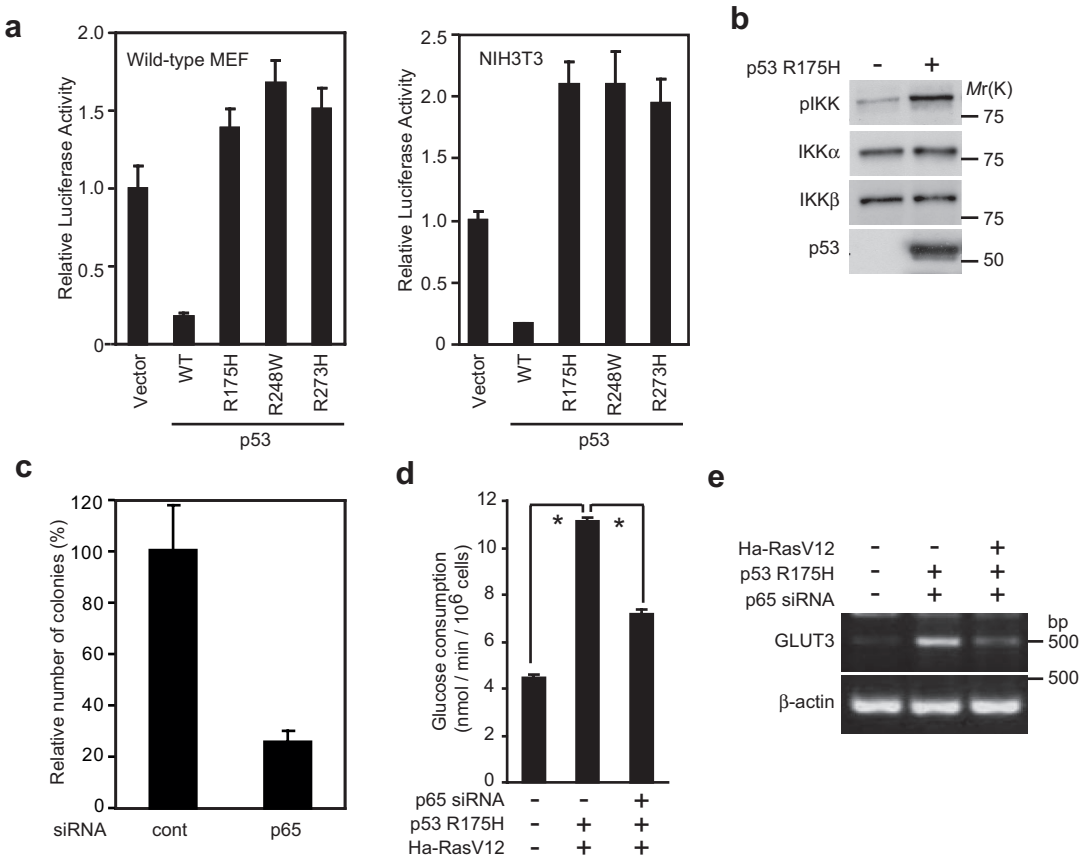

Figure S4 Enhanced glycolysis and *GLUT3* expression in Ha-Ras-V12-expressing wild-type MEFs by p53 mutants are suppressed by p65-knockdown. **(a)** Wild-type p53 (WT)- or mutant p53 (R175H, R248W or R273H)-expression vectors were cotransfected with the NF-κB Luc reporter plasmid and phRL-TK into wild-type MEFs (left panel) or NIH3T3 cells (right panel). After 24 h from transfection, relative luciferase activity was evaluated. **(b)** Wild-type MEFs were infected with a p53 R175H-expressing retrovirus. Phosphorylation of IKKα/β was determined by immunoblot analysis with an anti-phospho-IKK (pIKK) antibody. **(c-e)** Wild-type MEFs were infected with a Ha-RasV12- and a p53 R175H-expressing retrovirus together with control- or p65 siRNA-expressing retroviruses. MEFs were subjected to colony formation assay **(c)**. Glucose consumption was measured **(d)**. *, $p < 0.01$ for indicated comparison (t-test). *GLUT3* gene expression was examined by RT-PCR **(e)**. In a, c and d, data are mean ±s.d. from three independent experiments.

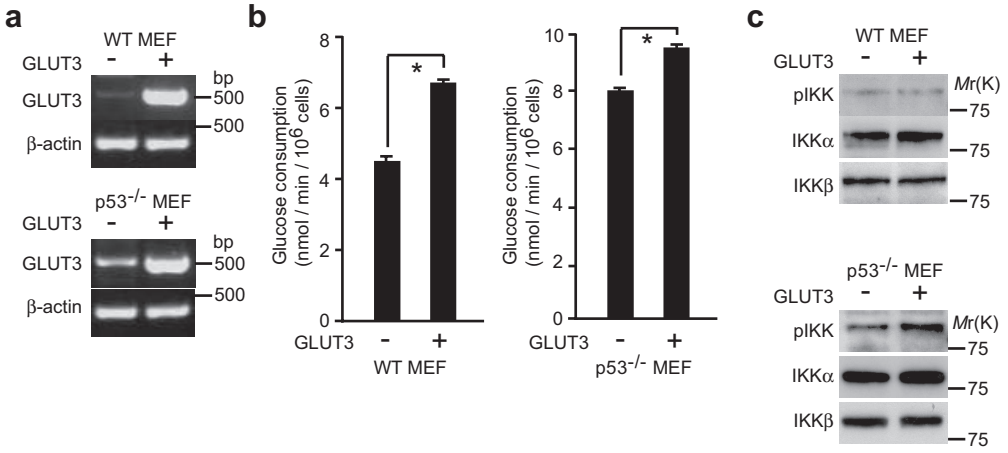

Figure S5 Exogenous GLUT3 enhances activation of IKK in *p53*$^{-/-}$ MEFs. **(a-c)** Wild-type or *p53*$^{-/-}$MEFs infected with control vector- or GLUT3 expressing-retrovirus. *GLUT3* gene expression was examined by RT-PCR **(a)**. Glucose consumption was measured **(b)**. Data are mean ±s.d. from three independent experiments. *, $p < 0.01$ for indicated comparison (t-test). Phosphorylation of IKKα/β was determined by immunoblot analysis with an anti-phospho-IKK (pIKK) antibody **(c)**.

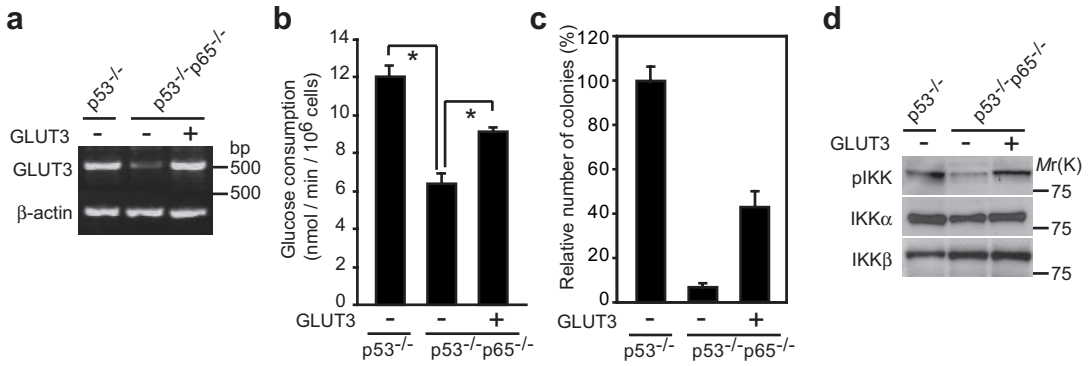

Figure S6 Exogenous GLUT3 restores colony formation and glucose consumption in Ha-Ras-V12-expressing *p53*$^{-/-}$*p65*$^{-/-}$MEFs. **(a-d)** Ha-RasV12-expressing *p53*$^{-/-}$*p65*$^{-/-}$MEFs were superinfected with control vector- or a GLUT3-expressing-retrovirus. *GLUT3* gene expression was examined by RT-PCR **(a)**. Glucose consumption was measured **(b)**. *, $p < 0.01$ for indicated comparison (t-test). MEFs were subjected to colony formation assay **(c)**. In b and c, data are mean ±s.d. from three independent experiments. Phosphorylation of IKKα/β was determined by immunoblot analysis with an anti-phospho-IKK (pIKK) antibody **(d)**.

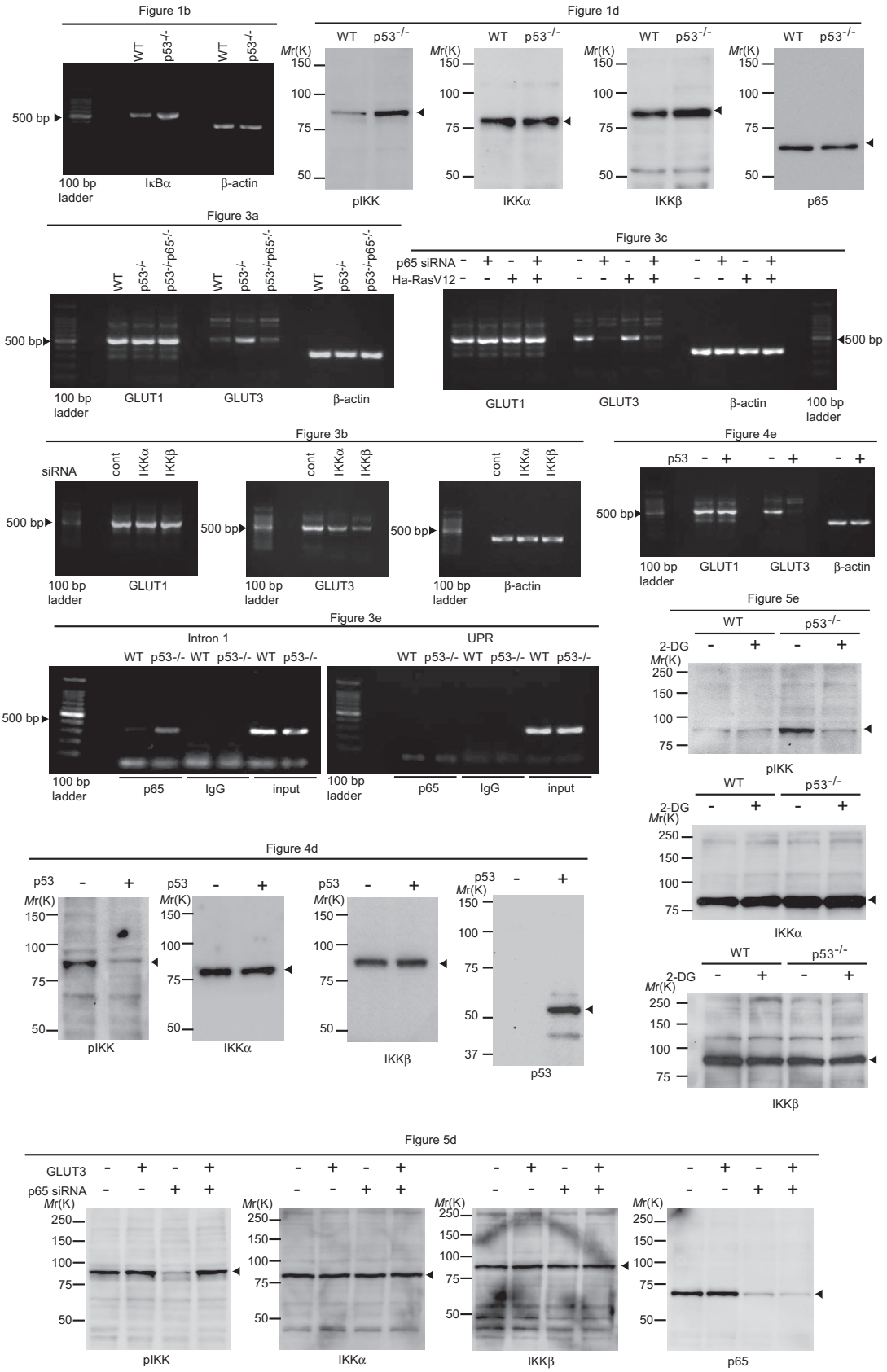

Figure S7 The panels of primary gels from figures indicated.